CrystEngComm

ROYAL SOCIETY OF CHEMISTRY

PAPER

View Article Online
View Journal | View Issue

Cite this: *CrystEngComm*, 2025, **27**, 7713

New forms of apremilast with halogen derivatives of benzoic acid

Yelizaveta Naumkina, [ab] Bohumil Kratochvíl,[a] Elena Korotkova[b] and Jan Čejka *[a]

Received 1st August 2025,
Accepted 13th October 2025

DOI: 10.1039/d5ce00770d

rsc.li/crystengcomm

Apremilast is a poorly soluble active pharmaceutical ingredient. It is prone to form multicomponent crystals and crystallizes in very similar molecular arrangements. We have crystallized apremilast with derivatives of halogen benzoic acid. Such compounds are known to moderate crystallization processes to different polymorphs of paracetamol. Surprisingly, apremilast structure packing was able to accommodate the *o*- and *m*-halogen benzoic acid derivatives in the same structure type as for known structures. On the other hand, crystallization with *p*-halogen benzoic acid derivatives leads to a cocrystal form with a rare molecular arrangement, which is likely less stable, and hence not preferred in the structures with smaller co-formers. The new forms were characterized by Single Crystal and Powder X-Ray Diffraction, and their stability was studied and compared by Differential Scanning Calorimetry and Thermogravimetric Analysis.

Introduction

Non-covalent interactions are significant in functional material formation.[1,2] These interactions allow for cocrystal creation and crystal engineering of the desired physicochemical characteristics of active pharmaceutical ingredients (APIs).[3] Properties, such as stability, hygroscopicity, and solubility, can be altered without changing the molecular structure of the API.[4]

A hydrogen bond network is typically the primary force driving the formation of crystalline multicomponent forms.[5] However, in some cases, other interactions, such as halogen bonds and π–π interactions, play a more dominant role.

Apremilast (APR) (Fig. 1) is an oral drug that inhibits PDE4 activity. Out of many known forms, form B, which is a thermodynamically stable anhydrous form, is used in the drug formulation.[6,7] In 2014, it was approved by the US Food and Drug administration for the treatment of psoriasis and PsA and in 2015 by the European Commission.[8] APR is used to treat adult patients with moderate to severe plaque psoriasis who have contraindications or are intolerant to other systemic therapies.[9] According to the Biopharmaceutical Classification System (BCS), APR belongs to the class IV type of drug (drugs with low solubility and low permeability).[10] Poor solubility is a significant issue for orally administered drugs. Multicomponent forms of APR showed high intrinsic dissolution rates compared to those of form B.[11,12] Thermal analysis of multicomponent forms has shown varying results from 107 °C (APR solvate with dichloromethane) to 189 °C (APR cocrystal with salicylic acid).[11–15,17] The melting points of some cocrystals (*e.g.* APR with nicotinamide,[13] cinnamic acid,[14] caffeine[12] and 4-hydroxybenzoic acid[13]) and solvates (*e.g.* APR with dichloromethane, ethyl acetate, pyridine)[18] were lower than the APR melting point (158 °C),[17] in contrast to APR solvates (*e.g.* APR with toluene[18]) and cocrystals (*e.g.* APR with phthalic acid,[14] and salicylic acid[14]) with slightly higher melting points. While APR form B crystallizes in a monoclinic $P2_1$ space group, the structures of the multicomponent forms share the same structure type, held together by π–π interactions, in the tetragonal $P4_12_12$ space group. The APR cocrystal with cinnamic acid crystallizes in the orthorhombic $P2_12_12_1$ space group.[11–18]

Halogen derivatives of benzoic acid have drawn our attention because of their ability to selectively control the paracetamol polymorphism. The sole presence of dissolved halogen benzoic acids in the mother liquor led to spontaneous crystallization of paracetamol form II instead of form I.[19] The halogen substitution of the benzoic ring has an impact on molecular packing in cocrystals.[20–24] The midplane distance of the acridine framework increases with the halogen substituent size.[24] The substituent position affects the type, strength, and number of intermolecular bonds in acridine cocrystals with halogen benzoic acid (HBA), and hence it affects the stability and melting temperature of the products.[20]

We investigated the impact of halogen benzoic acid derivatives on the crystal packing of the APR forms. A series

[a] *Department of Solid-State Chemistry, University of Chemistry and Technology, Technická 5, 166 28 Prague 6 – Dejvice, Czech Republic. E-mail: cejkaj@vscht.cz*
[b] *Department of Physical Analytical Chemistry, National Research Tomsk Polytechnic University, Lenina Avenue, 30, 634050, Tomsk, Russia*

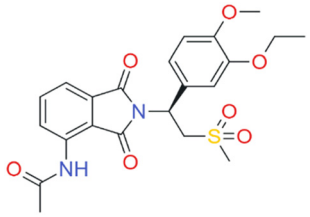

Fig. 1 Molecular structure of apremilast.

of benzoic acid derivatives was inspected, as variable effectivity of paracetamol form II crystallization depending on various derivatives was reported. We expected crystallization of new forms, as well as the possibility of incorporation of halogen benzoic acid derivatives into the APR structure. Our further research aimed to examine APR solid forms with five similar coformers and to explore how the position of substituents in the coformer affects the structural and physicochemical properties of the resulting solid forms.

Experimental

Five halogen derivatives of benzoic acid (2-chlorobenzoic acid, 3-chlorobenzoic acid, 4-chlorobenzoic acid, 3-bromobenzoic acid and 4-bromobenozoic acid) were chosen to find new forms of APR, preferably new polymorphs. To our surprise, the benzoic acid derivatives not only failed to induce crystallization of new polymorphs, but also were prone to enter the structure of APR, thus creating a distinctive series of cocrystals.

Materials

Commercially available compounds were used without further purification. The solvents were analytical and chromatographic grade purity, apremilast (form B) was provided by the pharmaceutical company Zentiva; 2-chlorobenzoic acid, 98%, 3-chlorobenzoic acid, 99+%, 4-chlorobenzoic acid, 99%, and 4-bromobenzoic acid, 97%, were obtained from Acros Organics Ltd., Belgium; 3-bromobenzoic acid, 99%, was obtained from ThermoFisher Scientific Co. Ltd., Brno, Czech Republic. Distilled water was used for experiments.

Cocrystal synthesis and single crystal preparation

Slow solvent evaporation from a solution of APR and a coformer was used for the synthesis of the cocrystals. Various solvents were used: ethanol, methanol, acetone and methyl ethyl ketone (MEK). The solvents were selected based on the solubility of the raw materials and the application of solvents in the pharmaceutical industry. The results of the cocrystal growth experiments are summarized in Table 1. Suitable samples for further studies were crystallized from solutions of APR and coformers dissolved in MEK in a 2 : 1 ratio. In the case of APR:4-BrBA, the solution was heated up at 40 °C for 3 hours. After 4–5 days, transparent crystals of the APR cocrystal with 4-BrBA were obtained for further study.

Table 1 Results of cocrystal preparation by different methods

	Molar ratio							
Coformer	1 : 1	2 : 1	1 : 1	2 : 1	1 : 1	2 : 1	1 : 1	2 : 1
2-ClBA	✗	✗	✓	✓	✓	✓	✓	✓
3-ClBA	✗	✗	✓	✓	✗	✗	✓	✓
4-ClBA	✗	✗	✓	✓	✗	✗	✓	✓
3-BrBA	✗	✗	✗	✗	✓	✓	✓	✓
4-BrBA	✗	✗	✓	✓	✗	✗	✓	✓
Solvent	Methanol		Ethanol		Acetone		MEK	

✓ – new solid forms obtained, ✗ – mixture of APR and coformers.

APR:2-ClBA

150 mg (0.3254 mmol) of APR and 25.5 mg (0.01629 mmol) of 2-chlorobenzoic acid were dissolved in methyl ethyl ketone (MEK) (5 ml). Bipyramidal white crystals were harvested under ambient conditions after 2–3 days. Mp – 177 °C.

APR:3-ClBA

150 mg (0.3254 mmol) of APR and 25.5 mg (0.01629 mmol) of 3-chlorobenzoic acid were dissolved in MEK (5 ml). Bipyramidal yellow crystals were harvested under ambient conditions after 2–3 days. Mp – 170 °C.

APR:4-ClBA

150 mg (0.3254 mmol) of APR and 25.5 mg (0.01629 mmol) of 4-chlorobenzoic acid were dissolved in MEK (5 ml). Bipyramidal yellow crystals were harvested under ambient conditions after 3–4 days. Mp – 147 °C.

APR:3-BrBA

150 mg (0.3254 mmol) of APR and 32.7 mg (0.0163 mol) of 3-bromobenzoic acid were dissolved in MEK (5 ml). Bipyramidal white crystals were harvested under ambient conditions after 3–4 days. Mp – 163 °C.

APR:4-BrBA

150 mg (0.3254 mmol) of APR and 32.7 mg (0.0163 mol) of 2-chlorobenzoic acid were dissolved in MEK (5 ml) and mixed for 3 hours at 40 °C. After 4–5 days, yellow bipyramidal crystals were obtained along with needle-shaped crystals of APR and 4-BrBA.

The obtained products were rinsed with MEK for further analyses.

Single crystal X-ray diffraction

X-ray diffraction patterns of suitable single crystals were collected on a Bruker D8 VENTURE system equipped with a charge-integrating pixel array detector Photon II 7 multilayer monochromator and a CuKα Incoatec microfocus sealed tube (λ = 1.54178 Å) using combined φ and ω scans at 180 K. Data

reduction and absorption correction by a multi-scan method were performed using Bruker software program – Apex4.[25] Structures were solved by SHELXT[26] and refined using Crystals software.[27] The coformer molecule was disordered over two-fold axes with 50% partial occupancy in the crystal structures of APR with 2-ClBA, 3-ClBA and 4-ClBA. Non-hydrogen atoms were refined anisotropically. Hydrogen atoms were located in the difference Fourier map and refined as riding; in APR:3-ClBA, the hydrogen atoms were refined as fixed. The hydrogen atoms attached to heteroatoms were placed geometrically, and their coordinates were refined with soft restraints on distance and U_{iso}. The crystallographic data for all structures have been deposited at the Cambridge Crystallographic Data Center (CCDC 2477189–2477193).

Powder X-ray diffraction (PXRD)

X-ray powder diffraction data were collected at room temperature using an X'Pert[3] Powder θ–θ diffractometer with the Bragg–Brentano parafocusing geometry using CuKα radiation (λ = 1.5418 Å, U = 40 kV, I = 30 mA) (Malvern Panalytical, Malvern, UK). An ultrafast detector PIXCEL was employed to collect XRD data over the angular range from 5 to 50° (2θ) with a step size of 0.039° 2θ, and a counting time of 0.706 s per step. Data evaluations were performed in the software package HighScore Plus 3.0.[28]

DSC

Differential scanning calorimetry (DSC) was performed on a DSC 131 (Setaram, France). Samples of APR:2-ClBA, APR:3-ClBA, APR:4-ClBA, and APR:3-BrBA were placed in aluminum pans with a lid for DSC. The temperature range was 5–250 °C at 10 °C min^{-1}. The melting points were established from peak onsets, without normalizing by the heating rate.

TGA

Thermogravimetric analysis was performed using a TGA5500 TA Instruments thermal analyzer. The sample of APR:4-ClBA was heated at 10 °C min^{-1} in a temperature range of 20–206 °C in aluminium oxide crucibles.

Results and discussion

Five new cocrystals of apremilast are reported. New polymorphs were not found. All crystal structures of the new forms were determined by single-crystal X-ray diffraction (SCXRD), and the theoretical powder X-ray diffraction (PXRD) patterns were similar to the experimental PXRD patterns of the bulk products. Physicochemical properties were evaluated by DSC and TGA.

Crystal structures of bipyramidal cocrystals of APR with 2-ClBA (2 : 1), 3-ClBA (2 : 1), 4-ClBA (2 : 1), 3-BrBA (2 : 1), and 4-BrBA (2 : 1) were solved by SCXRD, for parameters see Table S1 in the SI. Cocrystals of APR with 2-ClBA, 3-ClBA, and 3-BrBA crystallized in the tetragonal space group $P4_12_12$, while cocrystals of APR with 4-ClBA and 4-BrBA have grown in the orthorhombic space group $P2_12_12_1$. (Fig. 2). APR was reported crystallizing with coformers in tetragonal $P4_12_12$, and the coformers were approximately in the same position.[13,16,17] Only one non-isostructural APR cocrystal was

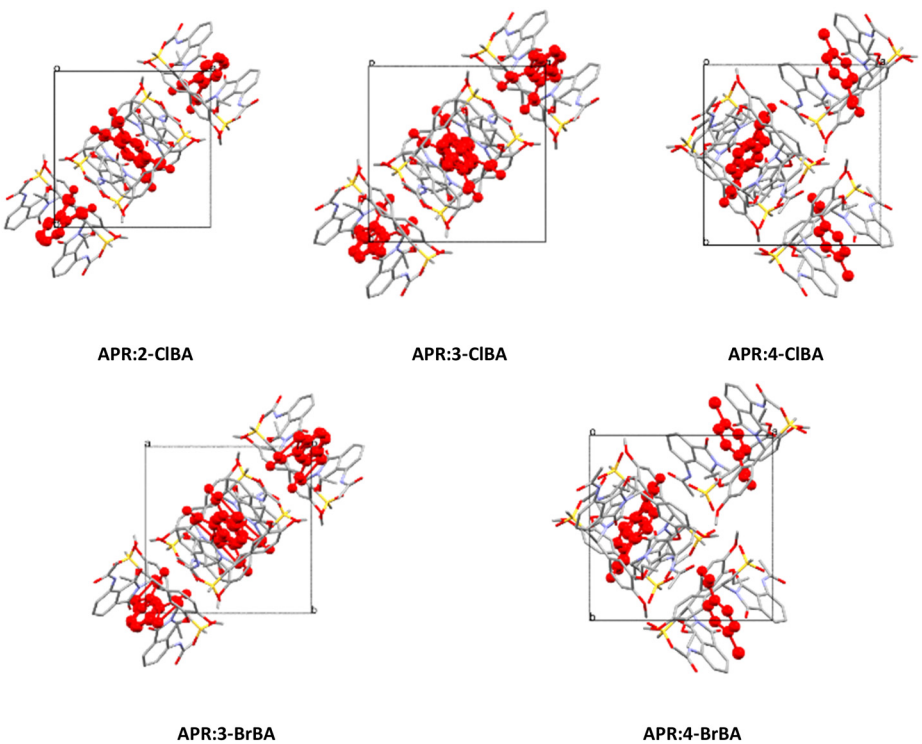

Fig. 2 Molecular packing of APR cocrystal structures along the c axis (coformers highlighted in red).

reported in orthorhombic $P2_12_12_1$.[14] We expected the refinement in lower symmetry instead of $P4_12_12$ to eliminate the coformer disorder. Structure solutions in $P4_1$, $P12_11$ and $P1$ did not resolve the disorder. Hence, the structure model was refined in $P4_12_12$. The solution in lower symmetry was, however, helpful to set up suitable models of the coformer disorder.

The *para*-position of a halogen substituent in 4-ClBA and 4-BrBA altered the packing, and hence the volume and unit cell parameters as well (Table S1). It is likely that the size (length) of the molecule couldn't be accommodated by the surrounding APR molecules.

Void space analysis

To evaluate various coformer steric demands, the void space analysis was performed using the Platon software[29] using the CALC VOIDS option with the solvent and coformer removed from the model. The volume of the void in the unit cell and packing index[30] for each cocrystal structure are presented in Table 2. The volume occupied by cinnamic acid in the APR cocrystal (APR:CA)[14] is even larger than the volumes occupied by *para*-halogen benzoic acids in APR:4-ClBA and APR:4-BrBA crystal structures. The APR:CA structure supports our theory that the coformer size determines the resulting cocrystal form.

Table 2 Analysis of coformer accessible voids

Structure	V_V, A^3	V_V/V, %	Packing index, %	V_m
APR:2-ClBA	211	16.9	60.8	2-ClBA
APR:3-ClBA	216	17.2	60.6	3-ClBA
APR:4-ClBA	224	17.6	59.1	4-ClBA
APR:3-BrBA	212	16.9	60.1	3-BrBA
APR:4-BrBA	231	18.0	58.3	4-BrBA
APR:CA[12]	241	18.5	58.1	CA

V_V – volume of the void in the unit cell, V_V/V – fraction of void volume per volume of the unit cell (%), packing Index and V_m – coformer in the void, CA – cinnamic acid.

Intermolecular interactions

APR molecules and coformer molecules interact with each other by weak intermolecular forces like hydrogen bonds, π–π interactions or van der Waals forces. Hydrogen bond network data presented in Table S2 were calculated using PLATON.[29] Coformer and APR molecules are held together by the hydrogen bond formed between the carboxyl group of the coformer and the ethoxy group in the APR molecule (Fig. 3). In the APR cocrystals with 4-BrBA and 4-ClBA, there is a three-centered hydrogen bond, where the H atom on the carboxyl group of coformers is hydrogen-bonded to both oxygen atoms in the ethoxy and methoxy groups in APR (Fig. 3(e and c)). Similar three-centered hydrogen bond interactions between the coformer and the APR molecule can be observed in the APR:CA[14] structure (Fig. S1). The formation of the three-center bond between the coformer and APR is likely triggered by the distance and orientation of

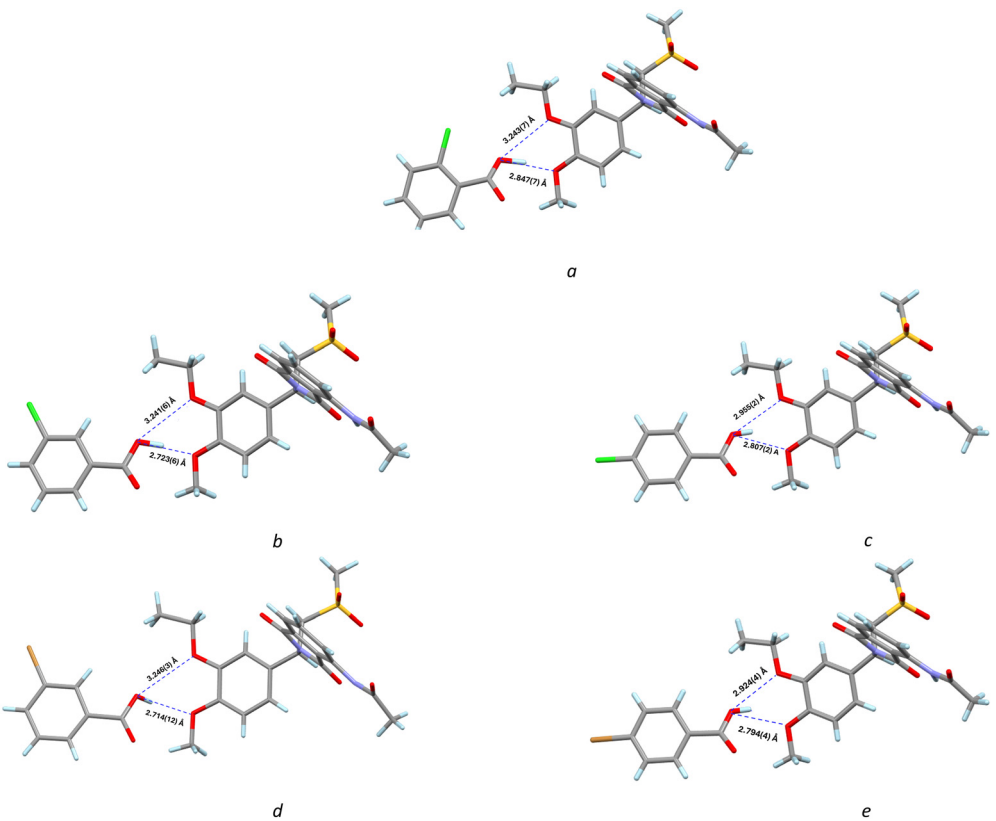

Fig. 3 D···A distances in the structure of a: APR:2-ClBA; b: APR:3-ClBA; c: APR:4-ClBA; d: APR:3-BrBA; e: APR:4-BrBA.

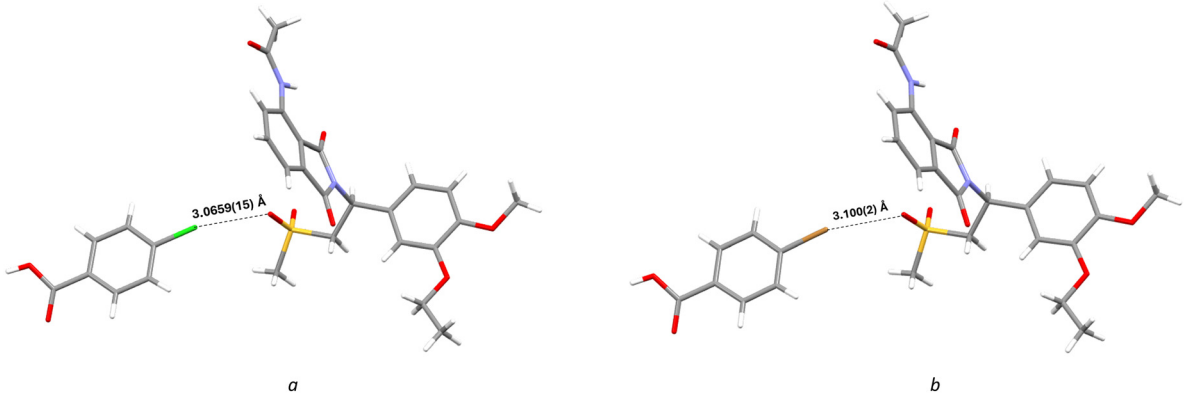

Fig. 4 Halogen bonds in the structure of a: APR:4-ClBA; b: APR:4-BrBA.

Table 3 The values of the nearest perpendicular distances of the coformer benzene ring on the plane of the APR phthalimide ring involved in the π–π interactions

Cocrystal	APR:2-ClBA	APR:3-ClBA	APR:4-ClBA	APR:3-BrBA	APR:4-BrBA
$d(\pi-\pi)$, Å	3.421/3.444	3.357/3.335	3.407/3.301	3.394/3.313	3.411/3.316
$<(\pi-\pi)$, °	1.68/1.83	5.02/6.10	5.02/7.47	5.14/6.70	5.46/7.84

the coformer, which depends on the position of the halogen substituent in the aromatic ring relative to the carboxyl group.

Besides hydrogen bonds, two cocrystals (APR:4-ClBA and APR:4-BrBA) form a halogen bond between the halogen atom in the coformer and the oxygen atom in the sulfonyl group of the APR molecule. APR:4-ClBA: d(O···Cl) = 3.0659(15) Å; APR:4-BrBA: d(O···Br) = 3.100(2) Å (Fig. 4).

APR–coformer–APR is bound by the π–π stacking, which is a distinct feature of the crystal structures of APR with various coformers, where the coformer molecules are almost parallel to the phthalimide ring in the APR molecule (Fig. S2). The shortest perpendicular distances of the coformer benzene ring to the plane of the phthalimide ring involved in the π–π interactions are presented in Table 3. In the series APR:3-ClBA – APR:3-BrBA and APR:4-ClBA – APR:4-BrBA, the interplanar angle increases due to the increasing steric demands of the coformer molecule.

Powder X-ray diffraction

PXRD was used to verify that the material obtained corresponds to the calculated pattern to assure purity and stability. The formation of cocrystals was confirmed by PXRD analysis by comparing the diffraction pattern of the cocrystals with the corresponding starting materials. All synthesized cocrystals differ with respect to APR and coformers, indicating the likely formation of a new crystalline phase. The PXRD patterns of the cocrystal products APR:2-ClBA, APR:3-ClBA, and APR:3-BrBA are so similar to each other due to similar values of unit cell parameters (Fig. 5). PXRD patterns of APR:4-ClBA and APR:4-BrBA (see SI Fig. S3) are distinct from the previous ones despite similar unit cell parameters, because the structure and symmetry are different. All PXRD patterns along with theoretical patterns at 180 K are presented in the SI (Fig. S3).

DSC

Fig. 6 shows the DSC thermograms of APR and four new multicomponent crystals. The melting points (data were not normalized to account for the temperature rate) are presented in Table 4. The thermal analysis of APR:4-BrBA was not carried out due to the small quantity and low purity of the product.

On the DSC profile of APR:4-ClBA, there is a wide peak with two shoulders (Fig. S4d). The process is gently starting

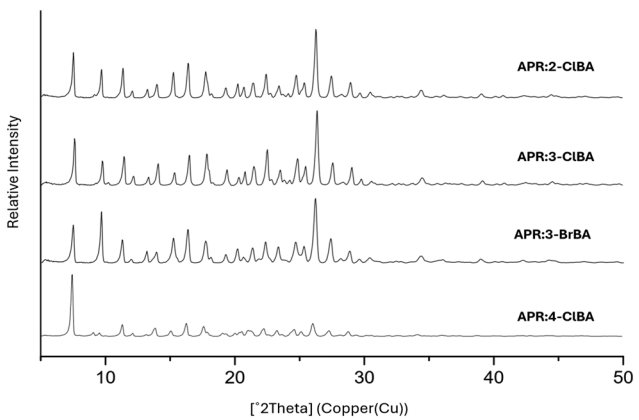

Fig. 5 PXRD patterns for the solid phases of APR with halogen derivatives of benzoic acids.

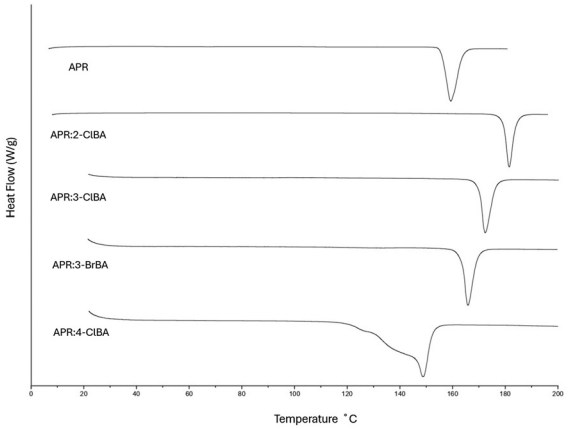

Fig. 6 DSC profiles of APR cocrystals.

Table 4 The melting point of starting material and cocrystals

Compound	t_m [°C]	Cocrystal APR:X-BA, t_m [°C]
APR	156[17]	—
2-ClBA	142[32]	177
3-ClBA	158[33]	170
4-ClBA	243[34]	147
3-BrBA	158[35]	163

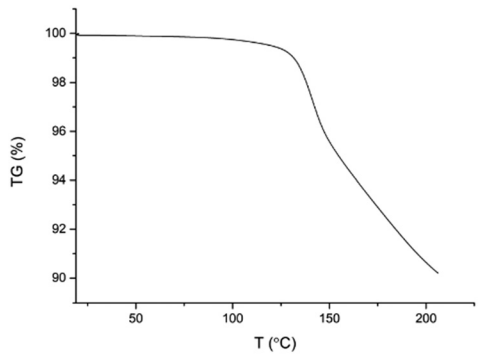

Fig. 7 TGA profile of the APR:4-ClBA cocrystal.

at approximately 118 °C. The peak maximum is at 147 °C. The TGA profile (Fig. 7) shows two degradation stages. At the first step at 100 °C, a mass loss of 0.02% of the original mass of 5.307 mg corresponds to residual solvent. The PXRD pattern of the product was analyzed after heating the material for 5 minutes at temperatures of 110 °C, 120 °C, 130 °C and 140 °C to investigate the changes occurring in the crystal structure. The analysis showed (Fig. S5) that the crystalline structure appeared intact, although the mass loss of the material is approx. 1.7% in each step (Fig. 7). At the second stage, the mass loss is about 3.6% at a temperature of about 175 °C, which probably indicates the process of decomposition of 4-ClBA. According to the DTA thermal stability study of 4-ClBA, the initial endothermic decomposition is caused by the dehydroxylation of the substance.[31]

The values of the melting points indicate that the thermal stability decreased in the order APR:2-ClBA > APR:3-ClBA > APR:4-ClBA. Such behavior corresponds to the stability estimations based on the packing index and hydrogen bond network comparison. Similar behavior was observed in the series of APR with *o*-xylene (182 °C),[14] *m*-xylene (166 °C)[13] and *p*-xylene (151 °C),[13] with the distance of the substituent in the aromatic ring. In contrast, there is a slight increase in the melting point with a decrease in the radius and electronegativity of the halogen substituent in the aromatic ring in the series of cocrystals with halogen derivatives of benzene (fluorobenzene (155 °C),[14] chlorobenzene (161 °C),[13] bromobenzene (163 °C),[13] and iodobenzene (162 °C)[13]). Meanwhile, in the series of APR:3-ClBA (170 °C) and APR:3-BrBA (163 °C), the melting point decreases slightly.

Crystal structure similarity

CrystalCMP rev.11[36] was applied to compare crystal structures of APR with halogen substituted benzoic acids. This method is based on a distance-displacement and angle-displacement comparison of molecules in a molecular cluster, where only larger molecules in the crystal structure are compared, which is the APR molecules, excluding coformers. The similarity parameter (P_{ab}) in the similarity matrix (Table 5) has a low value close to zero, which demonstrates the high similarity of structures between all five structures. Surprisingly, the dendrogram (Fig. S6 in the SI) revealed the high similarity of the new $P4_12_12$ and $P2_12_12_1$ APR cocrystal structures. The dendrogram of all known APR cocrystal structures demonstrates high similarity of the structures as shown in Fig. S7 in the SI. The similarity matrices for all published APR cocrystal structures are presented in SI2.

Table 5 Similarity matrix of the crystal structures of APR with halogen derivatives of benzoic acid

	APR:2-ClBA	APR:3-ClBA	APR:4-ClBA	APR:3-BrBA	APR:4-BrBA
	0	1	2	3	4
0: APR:2-ClBA	0.0000	0.1119	0.4091	0.0962	0.5440
1: APR:3-ClBA	0.1119	0.0000	0.3900	0.0702	0.5041
2: APR:4-ClBA	0.4091	0.3900	0.0000	0.4162	0.1003
3: APR:3-BrBA	0.0962	0.0702	0.4162	0.0000	0.4977
4: APR:4-BrBA	0.5440	0.5041	0.1003	0.4977	0.0000

Conclusion

Five new solid forms of apremilast cocrystals with halogen derivates of benzoic acid were prepared and fully characterized. Smaller coformers were adopted within the most abundant tetragonal form $P4_12_12$. Although the apremilast structure was able to accommodate all coformers, *para*-halogenated benzoic acid derivatives were too large resulting in structure symmetry decrease. Two cocrystal forms were prepared and characterized in the orthorhombic $P2_12_12_1$. Based on the crystal packing and melting point data, the tetragonal forms exhibited greater stability. Interestingly, no cocrystal disorder was observed in the less stable forms. The higher symmetry of the coformer may also have contributed to this behavior. Surprisingly, the high range of melting points of the coformers had no impact on the melting points of the cocrystals. In addition, higher stability of the tetragonal packing was demonstrated in comparison with the orthorhombic forms. The crystallization of novel apremilast polymorphs was not observed in the presence of benzoic acid derivatives.

Author contributions

J. Č. and E. K. conceived and supervised the project. Y. N. performed the investigation, data collection and analyses, Y. N. wrote the manuscript. J. Č. wrote, reviewed and edited the manuscript. All authors read the article and have given approval to the final version of the manuscript.

Conflicts of interest

There are no conflicts to declare.

List of abbreviations

APR	Apremilast
2-ClBA	2-Chlorobenzoic acid
3-ClBA	3-Chlorobenzoic acid
4-ClBA	4-Chlorobenzoic acid
3-BrBA	3-Bromobenzoic acid
4-BrBA	4-Bromobenzoic acid
MeOH	Methanol
EtOH	Ethanol
MEK	Methyl ethyl ketone
PXRD	Powder X-Ray Diffraction
SCXRD	Single Crystal X-Ray Diffraction
DSC	Differential Scanning Calorimetry

Data availability

Supplementary information is available. See DOI: https://doi.org/10.1039/d5ce00770d.

CCDC 2477189–2477193 (APR:2-ClBA, APR:3-ClBA, APR:4-ClBA, APR:3-BrBA and APR:4-BrBA) contain the supplementary crystallographic data for this paper.[37a–e]

Acknowledgements

This research was funded by the Czech Science Foundation Grant No. 21-05926X. The authors acknowledge the Central Laboratories of UCT, Prague for providing DSC and PXRD analyses.

Notes and references

1 J. B. David and W. S. Jonathan, Pharmaceutical cocrystals, salts and multicomponent systems; intermolecular interactions and property-based design, *Adv. Drug Delivery Rev.*, 2017, **117**(1), 3–24, DOI: 10.1016/j.addr.2017.03.003.

2 N. Gong, Y. Zhang, Y. Wang, H. Yu, B. Zhang, H. Zhang, Y. Lu and G. Du, Versatile salts as a strategy to modify the biopharmaceutical properties of venlafaxine and a potential hypoglycemic effect study, *Cryst. Growth Des.*, 2020, **20**, 3131–3139, DOI: 10.1021/acs.cgd.0c00007.

3 R. Ramalingam Sangeetha, K. Kasthuri Balasubramani, K. Kaliyaperumal Thanigaimani, J. S. Kavitha and M. Hemamalini, Co-crystal structures of 2,4-diamino-6-phenyl-1,3,5-triazine – 4-chlorobenzoic acid/4-methoxybenzoic acid: Synthesis, structural and Hirshfeld surface analysis, *Mol. Cryst. Liq. Cryst.*, 2018, **668**(1), 105–117, DOI: 10.1080/15421406.2019.1577485.

4 X. Gao, Z. Lin and S. Jin, *et al.*, Crystal and Molecular Structure of Four Organic Salts Assembled from Cyclohexylamine and Organic acids, *J. Chem. Crystallogr.*, 2014, **44**, 210–219, DOI: 10.1007/s10870-014-0503-9.

5 S. Allu, K. Suresh, G. Bolla, M. K. C. Mannava and A. Nangia, Role of Hydrogen Bonding in Cocrystals and Coamorphous Solids: Indapamide as a Case Study, *CrystEngComm*, 2019, **21**, 2043–2048, DOI: 10.1039/C8CE01075G.

6 M. Oracz, P. Garczarek, P. Skoczen, D. Podwysocka, M. Sculc and A. Majewski, WO2017/196192A1, Zaklady Farmaceutyczne Polpharma SA, World International Property Organization, 2017, p. 91, Available from: https://patents.google.com/patent/WO2017196192A1/en.

7 W. G. Muller, H. P. Schafer, H. Man, C. Ge and J. Xu, EP2276483B1, Celgene Corporation Summit, 2014, Available from: https://patents.google.com/patent/EP2276483B1/en.

8 P. Gisondi and G. Girolomoni, Apremilast in the therapy of moderate-to-severe chronic plaque psoriasis, *Drug Des., Dev. Ther.*, 2016, **10**, 1763–1770, DOI: 10.2147/dddt.s108115.

9 W. Baumer, J. Hoppmann, C. Rundfeldt and M. Kietzmann, Highly selective phosphodiesterase 4 inhibitors for the treatment of allergic skin diseases and psoriasis, *Inflammation Allergy: Drug Targets*, 2007, **6**, 17–26, DOI: 10.2174/187152807780077318.

10 P. Kulkarni and A. Deshpande, Analytical methods for determination of apremilast from bulk, dosage form and biological fluids: A critical review, *Crit. Rev. Anal. Chem.*, 2020, **51**, 258–267, DOI: 10.1080/10408347.2020.1718481/.

11 Y.-D. Wu, X.-L. Zhang, X.-H. Liu, J. Xu, M. Zhang, K. Shen, S.-H. Zhang, Y.-M. He, Y. Ma and A.-H. Zhang, *Acta Crystallogr., Sect. C: Struct. Chem.*, 2017, **73**, 305–313, DOI: 10.1107/S2053229617002984.

12 F. Y. Wang, Q. Zhang, Z. Zhang, X. Gong, J. R. Wang and X. Mei, *CrystEngComm*, 2018, **20**, 5945–5948.
13 J. Jirát, M. Babor, L. Ridvan, E. Skořepová, M. Dušek and M. Šoóš, Structure–Property Relations of a Unique and Systematic Dataset of 19 Isostructural Multicomponent Apremilast Forms, *IUCrJ*, 2022, **9**, 508–515, DOI: 10.1107/S2052252522005577.
14 J. Jirát, V. Zvoníček, M. Babor, L. Ridvan, E. Skořepová, M. Dušek and M. Šoóš, Formation of the first Non-isostructural cocrystal of apremilast explained, *Cryst. Growth Des.*, 2020, **20**, 5785–5795, DOI: 10.1021/acs.cgd.0c00393.
15 M. K. Dudek, E. Wielgus, P. Paluch, J. Śniechowska, M. Kostrzewa, G. M. Day, G. D. Bujacz and M. J. Potrzebowski, Understanding the Formation of Apremilast Cocrystals, *Acta Crystallogr., Sect. B: Struct. Sci., Cryst. Eng. Mater.*, 2019, **75**, 803–814, DOI: 10.1107/S205252061900917X.
16 Y. Naumkina, B. Kratochvíl, E. Korotkova and J. Čejka, Apremilast Cocrystals with Phenolic Coformers, *Molecules*, 2024, **29**, 6060, DOI: 10.3390/molecules29246060.
17 J. Jirát, D. Ondo, M. Babor, L. Ridvan and M. Šoóš, Complex Methodology for Rational Design of Apremilast-Benzoic Acid Co-Crystallization Process, *Int. J. Pharm.*, 2019, **570**, 118639, DOI: 10.1016/j.ijpharm.2019.118639.
18 M. K. Dudek, M. Kostrzewa, P. Paluch and M. J. Potrzebowski, pi-Philic Molecular Recognition in the Solid State as a Driving Force for Mechanochemical Formation of Apremilast Solvates and Cocrystals, *Cryst. Growth Des.*, 2018, **18**, 3959–3970, DOI: 10.1021/acs.cgd.8b00301.
19 L. H. Thomas, C. Wales, L. Zhao and C. C. Wilson, Paracetamol form II: An elusive polymorph through facile multicomponent crystallization routes, *Cryst. Growth Des.*, 2011, **11**, 1450–1452, DOI: 10.1021/cg2002018.
20 K. Kowalska, D. Trzybiński and A. Sikorski, Influence of the Halogen Substituent on the Formation of Halogen and Hydrogen Bonding in Co-Crystals Formed from Acridine and Benzoic Acids, *CrystEngComm*, 2015, **17**, 7199–7212, DOI: 10.1039/C5CE01321F.
21 L. Fotović, N. Bedeković, K. Pičuljan and V. Stilinović, Order versus Disorder in the Cocrystals of m-Halogenopyridines with m-Halogenobenzoic Acids: The Effects of the I···O Halogen Bond, *Cryst. Growth Des.*, 2022, **22**(12), 7508–7517, DOI: 10.1021/acs.cgd.2c01055.
22 J. Lombard, T. le Roex and D. A. Haynes, Competition between Hydrogen and Halogen Bonds: The Effect of Solvent Volume, *Cryst. Growth Des.*, 2020, **20**, 7384–7391, DOI: 10.1021/acs.cgd.0c01054.
23 A. Mirocki and A. Sikorski, Influence of Halogen Substituent on the Self-Assembly and Crystal Packing of Multicomponent Crystals Formed from Ethacridine and Meta-Halobenzoic Acids, *Crystals*, 2020, **10**, 79, DOI: 10.3390/cryst10020079.
24 F. M. A. Noa, S. A. Bourne, H. Su, E. Weber and L. R. Nassimbeni, Hydrogen bonding versus halogen bonding in host guest compounds, *Cryst. Growth Des.*, 2016, **16**, 4765–4771, DOI: 10.1021/acs.cgd.6b00886.
25 S. Bruker, *SAINT*, Bruker AXS Inc., Madison, WI, USA, 2002.
26 G. M. Sheldrick, SHELXT—Integrated Space-Group and Crystal-Structure Determination, *Acta Crystallogr., Sect. A: Found. Adv.*, 2015, **71**, 3–8, DOI: 10.1107/S2053273314026370.
27 P. W. Betteridge, J. R. Carruthers, R. I. Cooper, K. Prout and D. J. Watkin, CRYSTALS Version 12: Software for Guided Crystal Structure Analysis, *J. Appl. Crystallogr.*, 2003, **36**, 1487, DOI: 10.1107/S0021889803021800.
28 T. Degen, M. Sadki, E. Bron, U. König and G. Nénert, The HighScore suite, *Powder Diffr.*, 2014, **29**, S13–S18, DOI: 10.1017/S0885715614000840.
29 A. L. Spek, Single-crystal structure validation with the program PLATON, *J. Appl. Crystallogr.*, 2003, **36**, 7–13, DOI: 10.1107/S0021889802022112.
30 A. I. Kitaigorodskii, in *Molecular crystals and molecules*, ed. A. I. Kitaigorodsky, Academic Press, New York, 1973.
31 D. S. El Sayed and S. Foro, X-Ray Structure, DFT Study of p-Chlorobenzoic Acid, and the Effect of In Silico Molecular Docking on Tankyrase I Enzyme, *Russ. J. Bioorg. Chem.*, 2020, **46**, 542–550, DOI: 10.1134/S1068162020040184.
32 2-Chlorobenzoic acid. CAS Common Chemistry. CAS, a division of the American Chemical Society, n.d., https://commonchemistry.cas.org/detail?ref=118-91-2, (retrieved 2025-05-20) (CAS RN: 118-91-2). Licensed under the Attribution-Noncommercial 4.0 International License (CC BY-NC 4.0).
33 3-Chlorobenzoic acid. CAS Common Chemistry. CAS, a division of the American Chemical Society, n.d., https://commonchemistry.cas.org/detail?cas_rn=535-80-8, (retrieved 2025-05-20) (CAS RN: 535–80-8). Licensed under the Attribution-Noncommercial 4.0 International License (CC BY-NC 4.0).
34 4-Chlorobenzoic acid. CAS Common Chemistry. CAS, a division of the American Chemical Society, n.d., https://commonchemistry.cas.org/detail?cas_rn=74-11-3, (retrieved 2025-05-20) (CAS RN: 74–11-3). Licensed under the Attribution-Noncommercial 4.0 International License (CC BY-NC 4.0).
35 3-Bromobenzoic acid. CAS Common Chemistry. CAS, a division of the American Chemical Society, n.d., https://commonchemistry.cas.org/detail?cas_rn=585-76-2, (retrieved 2025-05-20) (CAS RN: 585–76-2). Licensed under the Attribution-Noncommercial 4.0 International License (CC BY-NC 4.0).
36 J. Rohlíček, E. Skořepová, M. Babor and J. Čejka, CrystalCMP: An easy-to-use tool for fast comparison of molecular packing, *J. Appl. Crystallogr.*, 2016, **49**, 2172–2183, DOI: 10.1107/S1600576716016058.
37 (*a*) CCDC 2477189: Experimental Crystal Structure Determination, 2025, DOI: 10.5517/ccdc.csd.cc2p4qbx; (*b*) CCDC 2477190: Experimental Crystal Structure Determination, 2025, DOI: 10.5517/ccdc.csd.cc2p4qcy; (*c*) CCDC 2477191: Experimental Crystal Structure Determination, 2025, DOI: 10.5517/ccdc.csd.cc2p4qdz; (*d*) CCDC 2477192: Experimental Crystal Structure Determination, 2025, DOI: 10.5517/ccdc.csd.cc2p4qf0; (*e*) CCDC 2477193: Experimental Crystal Structure Determination, 2025, DOI: 10.5517/ccdc.csd.cc2p4qg1.

